One-dimensional modeling of pulse wave for a human artery model

Masashi Saito 齋藤 雅史
Doshisha University, Kyoto, Japan

Supervisor: Pierre-Yves Lagrée - DR CNRS
Université Pierre et Marie-Curie
Institut Jean le Rond d'Alembert, Paris, France

September 27, 2010

Contents

List of Figures

List of Tables

Nomenclature

u	longitudinal velocity
u_0	velocity at the center of the tube
v	transversal velocity
h	thickness of the viscoelastic tube
h_0	unperturbed thickness of the viscoelastic tube
p	pressure
p_0	initial pressure
δp	unperturbed pressure
x	longitudinal variable
r	radial transversal variable
t	time
T_0	unperturbed time
R	tube radius
R_0	unperturbed tube radius
α	Womersley number
ω	angular frequency
ρ	density
K	volume elasticity of the tube wall
K_0	unperturbed volume elasticity of the tube wall
E_{est}	estimated elasticity of the tube wall
E_{msr}	measured elasticity of the tube wall
c	propagation velocity of the fluid
Q	flux
Q_0	unperturbed flux
A	cross section of the tube
A_0	unperturbed cross section of the tube
ν	dynamic coefficient of viscosity
τ	relaxation time
ε	$\delta R/R$
ε_p	coefficient of the nonlinear stress strain characteristics
L_0	longitudinal scale
J_0	Bessel function of order 0

1 Introduction

Arteriosclerosis is a vascular disease that leads to cardiovascular disease and stroke. The approach for diagnosing arteriosclerosis uses ultrasonography and magnetic resonance assessment to check the blood flow, blood pressure, and the displacement of vessel wall. Therefore, the study of the fluid dynamics in human artery is important.

After this introduction, in section 2, a short review of fluid dynamics in rigid and flexible tubes is given. This includes the discussion of the wave profiles owing to the Womersley numbers and the derivation of the governing equations for flow simulation in the flexible tube.

An important part, section 3, describes the first comparison between the measured and simulation data. We will measure the pressures propagating in the viscoelastic tube with different elastic moduli. Then non-dimensional equations are derived using limiting values of the non-dimensional parameters for the simple technique. The characteristics of wave propagation including attenuation and the velocity are evaluated by changing the parameters. The accuracy of the one-dimensional models are next checked by the powerful software COMSOL.

In section 4, we introduce the non-dimensional governing equations for the flow simulation in the tube with different characteristics and the bifurcation tube.

Fnally in section 5 a simple human artery model is described. The details of measurement and simulation techniques will be shown. Then we evaluate the utility of the simulation model by comparing the results.

2 Basic equations

This section explains the incompressible Navier-Stokes equations for the simulation of fluid dynamics in various tubes.

2.1 Flow dynamics in a rigid tube

The Navier-Stokes equations in a cylindrical coordinate system are used for governing equations [1].

$$\frac{1}{r}\frac{\partial}{\partial r}(rv) + \frac{\partial u}{\partial x} = 0 \tag{1}$$

$$\frac{\partial u}{\partial t} + u\frac{\partial u}{\partial x} + v\frac{\partial u}{\partial r} = -\frac{1}{\rho}\frac{\partial p}{\partial x} + \nu\left(\frac{1}{r}\frac{\partial}{\partial r}\left(r\frac{\partial u}{\partial r}\right) + \frac{\partial^2 u}{\partial x^2}\right) \tag{2}$$

$$\frac{\partial v}{\partial t} + u\frac{\partial v}{\partial x} + v\frac{\partial u}{\partial r} = -\frac{1}{\rho}\frac{\partial p}{\partial r} + \nu\left(\frac{\partial}{\partial r}\left(\frac{1}{r}\frac{\partial (rv)}{\partial r}\right) + \frac{\partial^2 v}{\partial x^2}\right), \tag{3}$$

where terms ν, ρ and p are the dynamic viscosity, the density and the pressure, respectively. The first equation is the equation of continuity for the incompressible fluids. The velocity is defined as $\mathbf{V} = u\mathbf{e_r} + v\mathbf{e_x}$. The second and third equations are the momentum transport equations. The volume force field such as gravity is ignored. Here, considering fully developed Newtonian flow in the rigid tube, the velocity v and the derivation of the velocity u become zero. These assumptions yield:

$$\frac{\partial u}{\partial x} = 0 \tag{4}$$

$$\frac{\partial u}{\partial t} = -\frac{1}{\rho}\frac{\partial p}{\partial x} + \nu\left(\frac{1}{r}\frac{\partial}{\partial r}\left(r\frac{\partial u}{\partial r}\right)\right) \tag{5}$$

$$\frac{\partial p}{\partial r} = 0. \tag{6}$$

It is nearly the case in the arteries where the wave length is very long compared to the tube radius (as it will be shown after). With regard to eqs. 4 and 6, we will assume a harmonic pressure and flow velocity and will search for harmonic solutions.

$$p = p_0 + p(x,t) = p_0 + p(x)e^{i\omega t} \qquad u = u(r,t) = u(r)e^{i\omega t}.$$

Then we define dimensionless variables for a simple technique:

$$r = R_0\bar{r} \qquad x = L_0\bar{x} \qquad t = \omega_0\bar{t} \qquad p(x) = p_0 + \delta p\bar{p}$$
$$u(r) = u_0\bar{u}\,,$$

where constants R_0, L_0, ω_0, δp, and u_0 are maximum value of each dimensional variable. Non-dimensional variables $\bar{r}$, $\bar{x}$, $\bar{t}$, $\bar{p}$, and $\bar{u}$ are in the range from 0 to 1.0. Substituting of these variables into eq. 5 yields:

$$i\bar{u} = -\frac{\delta p}{\rho\omega u_0}\frac{\partial\bar{p}}{\partial\bar{x}} + \frac{1}{\alpha^2}\frac{1}{\bar{r}}\frac{\partial}{\partial\bar{r}}\left(\bar{r}\frac{\partial\bar{u}}{\partial\bar{r}}\right), \tag{7}$$

with α, which is the Womersley number defined as:

$$\alpha = R_0\sqrt{\frac{\omega}{\nu}}. \tag{8}$$

The solution of eq. 7 is finally given by a Bessel equation:

$$\bar{u} = i\frac{\delta p}{\rho\omega u_0}\frac{\partial\bar{p}}{\partial\bar{x}}\left(1 - \frac{J_0(\bar{r}\alpha i^{\frac{3}{2}})}{J_0(\alpha i^{\frac{3}{2}})}\right). \tag{9}$$

Velocity profiles in radial direction at $t = 0$ are shown in Fig. 1. As shown in the figure, the velocity profiles change markedly depending on the Womersley number. We then derive approximate expressions in cases of small and large Womersley numbers.

Small Womersley number flow

If $\alpha \ll 1$, eq. 7 becomes:

$$0 = -\frac{\delta p}{\rho\omega u_0}\frac{\partial\bar{p}}{\partial\bar{x}} + \frac{1}{\alpha^2}\frac{1}{\bar{r}}\frac{\partial}{\partial\bar{r}}\left(\bar{r}\frac{\partial\bar{u}}{\partial\bar{r}}\right), \tag{10}$$

with boundary conditions $\bar{u}|_{\bar{r}=0}$ and $\dfrac{\partial\bar{u}}{\partial\bar{r}}|_{\bar{r}=0} = 0$. After surface integration, we obtain the approximate expression:

$$\bar{u} = -\frac{\alpha^2}{4}\frac{\delta p}{\rho\omega u_0}\frac{\partial\bar{p}}{\partial\bar{x}}(1-\bar{r}^2). \tag{11}$$

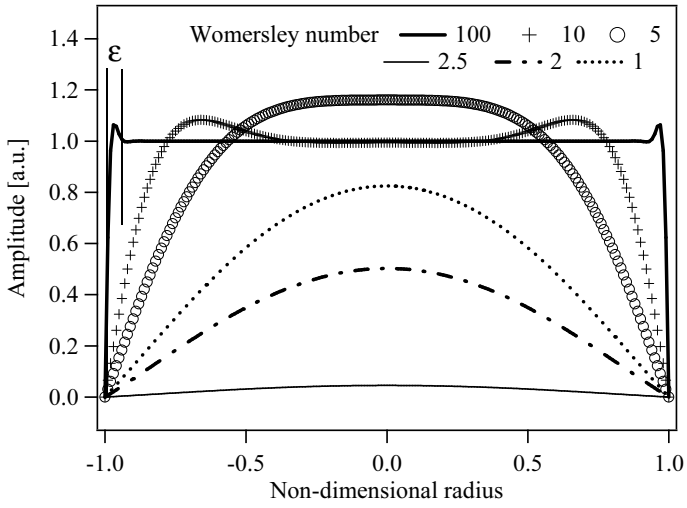

Fig. 1: Velocity profiles at different Womersley values.

for small α, we have a Poiseuille flow,
for large α, the profile becomes flat.

For small Womersley numbers, the parabolic profile which is called the Poiseuille profile is obtained.

Large Womersley number flow

Changing the variable $\bar{r} = 1 - \varepsilon\tilde{r}$, where ε represents the thin layer as shown in Fig. 1, the eq. 7 becomes:

$$i\tilde{u} = -\frac{\delta p}{\rho\omega u_0}\frac{\partial\bar{p}}{\partial\bar{x}} + \frac{1}{\alpha^2\varepsilon^2}\frac{\partial^2\tilde{u}}{\partial\tilde{r}}. \tag{12}$$

Since $\alpha \gg 1$ and $\varepsilon \ll 1$, we assume by dominant balance $\alpha\varepsilon = 1.0$. Substituting the relation, we obtain:

$$i\tilde{u} = -\frac{\delta p}{\rho\omega u_0}\frac{\partial\bar{p}}{\partial\bar{x}} + \frac{\partial^2\tilde{u}}{\partial\tilde{r}}, \tag{13}$$

with solution :

$$\bar{u} = i\frac{\delta p}{\rho\omega u_0}\frac{\partial \bar{p}}{\partial \bar{x}}\left(1 - e^{-\frac{\sqrt{2}}{2}(1+i)(1-\bar{r})\alpha}\right). \tag{14}$$

For large Womersley numbers, an oscillating flat flow profile is obtained in the core.

2.2 Flow dynamics in a flexible tube

Having some ideas on the possible shape of the velocity profiles, we turn now to the general case. It is impossible to have analytical solutions and numerical solution take a long time (as we will see with COMSOL). Thus we have to simplify the flow. Instead of using the full velocity field u and v, we will use a mean field (the mean longitudinal velocity or the flux) obtained by integration across the section.

For axisymmetric flow in a long flexible tube with small radius, the governing equations are given by [1]:

$$\frac{1}{r}\frac{\partial}{\partial r}(rv) + \frac{\partial u}{\partial x} = 0 \tag{15}$$

$$\frac{\partial u}{\partial t} + u\frac{\partial u}{\partial x} + v\frac{\partial u}{\partial r} = -\frac{1}{\rho}\frac{\partial p}{\partial x} + \frac{\nu}{r}\frac{\partial}{\partial r}\left(r\frac{\partial u}{\partial r}\right). \tag{16}$$

$$0 = -\frac{1}{\rho}\frac{\partial p}{\partial r} \tag{17}$$

We notice that the pressure does not change across the section, and that transverse viscous effects are negligible. We then derive one-dimensional equations from eqs. 15 and 16. After multiplying $2\pi r$, integration of both equations over the cross-sectional area yields:

$$\frac{\partial A}{\partial t} + \frac{\partial Q}{\partial x} = 0 \tag{18}$$

$$\frac{\partial Q}{\partial t} + \frac{\partial}{\partial x}\left(2\pi\int_0^R ru^2 dr\right) = -\frac{A}{\rho}\frac{\partial p}{\partial x} + 2\pi\nu\left[r\frac{\partial u}{\partial r}\right]_{r=R}, \tag{19}$$

where A is the cross section of the tube. The term Q is the flux defined as:

$$Q = \int_0^R 2\pi r u dr. \tag{20}$$

Here, the profile of flow velocity, which is a function of r, changes due to the Womersley number as expressed in section 2.1. We next derive governing equations for the velocity profiles with small and large Womersley numbers.

Small Womersley number flow

If α is small, the non-dimensional velocity profile is defined as eq. 11. Substituting eq. 11 into eq. 20 yields:

$$Q = \int_0^R 2\pi r u dr = -\frac{\pi\alpha^2}{8}\frac{\delta p}{\rho\omega}\frac{\partial \bar{p}}{\partial \bar{x}}R^2. \tag{21}$$

Thus, eq. 19 becomes:

$$\frac{\partial Q}{\partial t} + \frac{4}{3}\frac{\partial}{\partial x}\left(\frac{Q^2}{A}\right) = -\frac{A}{\rho}\frac{\partial p}{\partial x} - \frac{8\nu Q}{R^2}. \tag{22}$$

Large Womersley number flow

When α is large, the velocity profile almost becomes flat. Thus, the flux becomes:

$$Q = \frac{\delta p}{\rho\omega}\frac{\partial \bar{p}}{\partial \bar{x}}A. \tag{23}$$

Substituting eqs. 14 and 23 into eq. 19 yields:

$$\frac{\partial Q}{\partial t} + \frac{\partial}{\partial x}\left(\frac{Q^2}{A}\right) = -\frac{A}{\rho}\frac{\partial p}{\partial x} - \frac{\sqrt{2}\alpha\nu Q}{R^2}. \tag{24}$$

Governing equations

Finally, the governing equations for simulating the flow dynamics in a flexible tube are as follows.

Conservation of mass:

$$\frac{\partial A}{\partial t} + \frac{\partial Q}{\partial x} = 0$$

Momentum equation:

If $\alpha \ll 1$

$$\frac{\partial Q}{\partial t} + \frac{4}{3}\frac{\partial}{\partial x}\left(\frac{Q^2}{A}\right) = -\frac{A}{\rho}\frac{\partial p}{\partial x} - \frac{8\nu Q}{R^2}$$

If $\alpha \gg 1$

$$\frac{\partial Q}{\partial t} + \frac{\partial}{\partial x}\left(\frac{Q^2}{A}\right) = -\frac{A}{\rho}\frac{\partial p}{\partial x} - \frac{\sqrt{2}\alpha\nu Q}{R^2}.$$

3 Measurement and simulation of fluid dynamics in the straight tube

This section explains the difference between measurement and one-dimensional simulation results. We first measure pressures in a viscoelastic tube. Then we derive one-dimensional govering equations with non-dimensional variables and three tube laws to simulate the measured pressure waves. Finally, optimum fitting coefficients are decided.

3.1 Measurement

We measured the pressure waves in the viscoelastic tube with different elastic moduli. The measurement system used is shown in Fig. 2. It is constructed by a viscoelastic tube, tank, and pump (Custom made, Tomita engineering Co., Ltd). Three kinds of viscoelastic tubes (silicone, natural rubber and neoprene rubber, length 35.15 m, diameter 8 mm, thickness 2 mm) were used. The elasticities of each tube were about 1.3 MPa, 2.5 MPa, and 4.6 MPa by the tensile test. A pulse flow was input into the tube from the pump. Here, the input flow signal to the pump was a half cycle of a sinusoidal wave. The period was 0.3 s and the total flow volume was 4.5 ml. The input liquid used was water. Then we measured the inner pressure wave in the tube with intervals of 5 m using a pressure sensor (Keyence AP-10S).
Figures 3, 4, and 5 show the pressure waves in cases of natural, silicone and neoprene rubber tubes, respectively. On those figures, pressure is plotted as a function of time at the different points of measurement. We observe the increase and decrease of the pulse at the various positions. The marked differences were the amplitude of pressure waves and the propagation velocities. Since the velocity appeared to be proportional to the square root of Young's elastic moduli of vessel walls [2], the augmentation of the velocity was caused by the increase in elasticity of viscoelastic tube. In case of the pressure waves propagating in natural rubber, the velocity was so slow that the forward waves were only observed. On the other hand, the velocity of the pressure waves in silicone and neoprene rubber was fast compared with that of natural rubber. Thus reflected waves from the end of tube were confirmed. We next simulated the pressure wave and flux for better understanding of the fluid in these tubes.

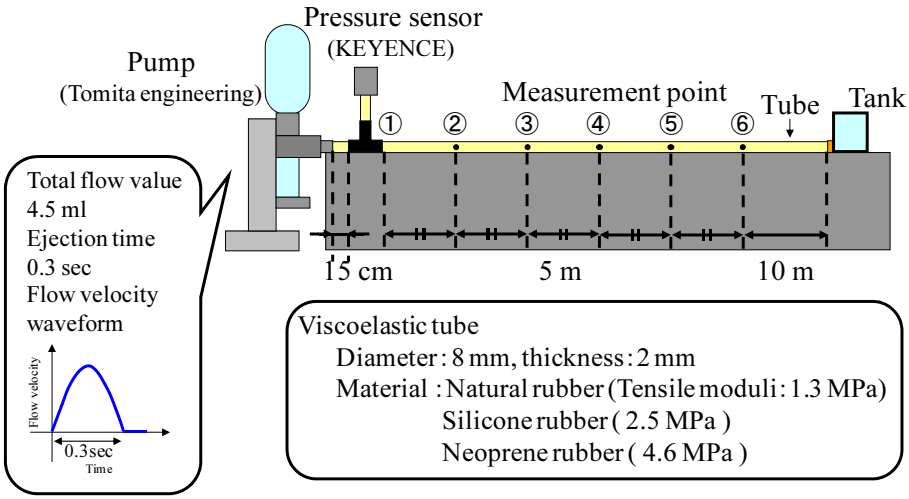

Fig. 2: Measurement system used.

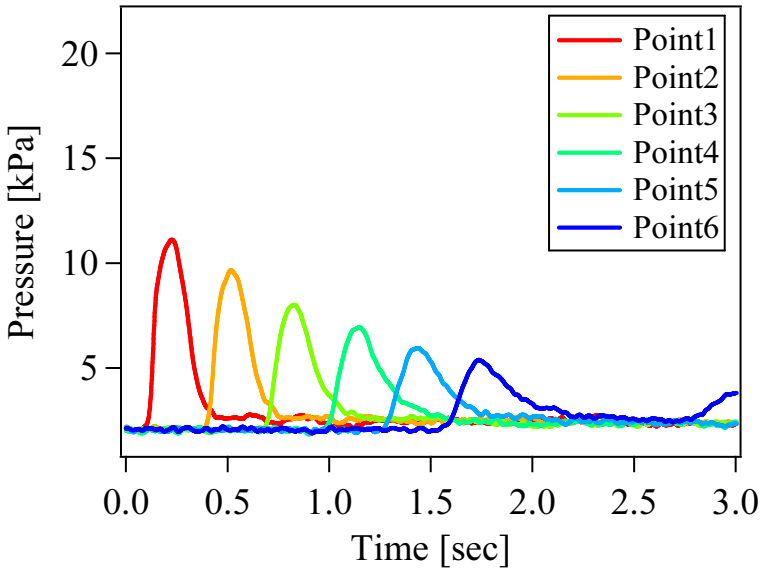

Fig. 3: Measured pressure waves (natural rubber tube).

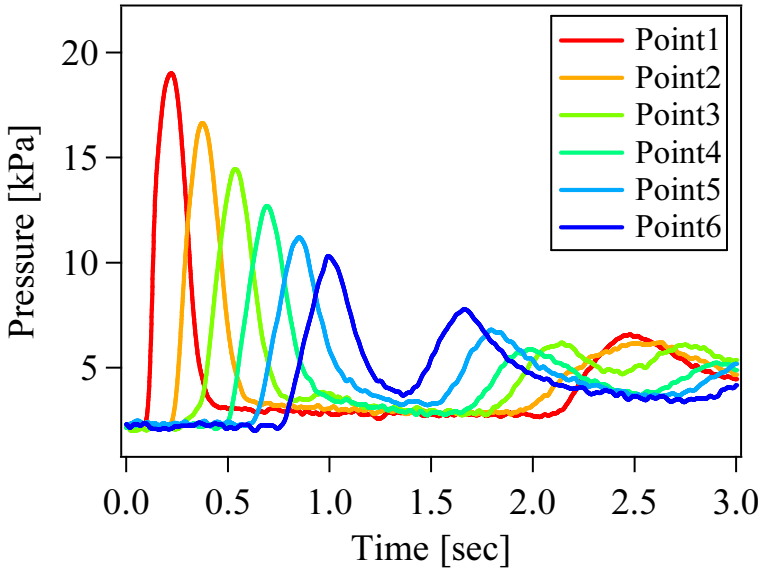

Fig. 4: Measured pressure waves (silicone rubber tube).

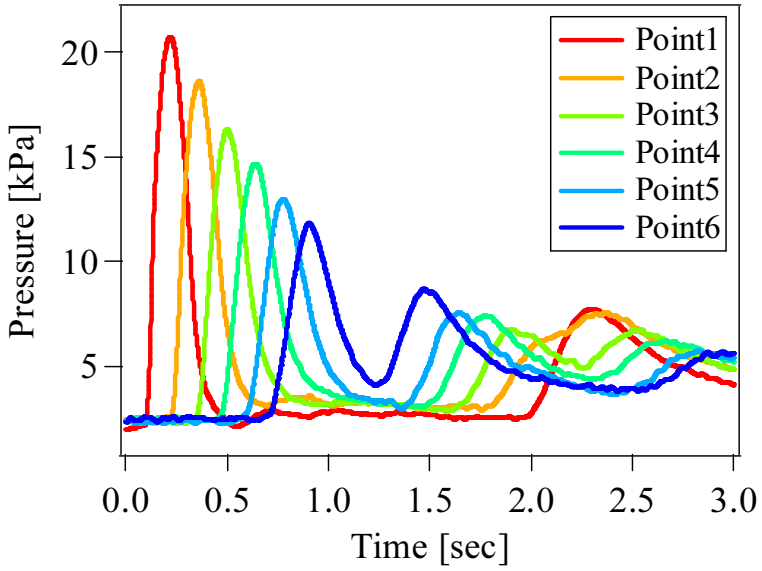

Fig. 5: Measured pressure waves (neoprene rubber tube).

3.2 Non-dimensional governing equations

Let us come back to the mathematical modelisation:

Conservation of mass:

$$\frac{\partial A}{\partial t} + \frac{\partial Q}{\partial x} = 0.$$

Momentum equation:

If $\alpha \ll 1$

$$\frac{\partial Q}{\partial t} + \frac{4}{3}\frac{\partial}{\partial x}\left(\frac{Q^2}{A}\right) = -\frac{A}{\rho}\frac{\partial p}{\partial x} - \frac{8\nu Q}{R^2}$$

If $\alpha \gg 1$

$$\frac{\partial Q}{\partial t} + \frac{\partial}{\partial x}\left(\frac{Q^2}{A}\right) = -\frac{A}{\rho}\frac{\partial p}{\partial x} - \frac{\sqrt{2}\alpha\nu Q}{R^2}.$$

Pressure law (elastic model):

$$P = P_0 + K(R - R_0).$$

We then derive the non-dimensional equations for a simple computation. Here, we define dimensional variables as follows.

$$t = T_0\bar{t} \qquad x = L_0\bar{x} = c_0T_0\bar{x} \qquad R = R_0 + \delta R\bar{R}$$
$$A = A_0\bar{A} = \pi R_0^2\left(1 + 2\frac{\delta R}{R_0}\bar{R}\right) \qquad Q = Q_0\bar{Q}$$

where constants T_0, L_0, δR, A_0, and Q_0 are maximum values of dimensional variables. Non-dimensional variables $\bar{t}$, $\bar{x}$, $\bar{R}$, $\bar{A}$, and $\bar{Q}$ are of order one, it means that they are in the range from 0 to not more than 1.0. Substitution of non-dimensional variables and the pressure law in governing equtions yields:

Conservation of mass:

$$\frac{\partial \bar{R}}{\partial \bar{t}} = -\frac{Q_0T_0}{2\pi R_0\delta R L_0}\frac{\partial \bar{Q}}{\partial \bar{x}}. \tag{25}$$

Momentum equation:

If $\alpha \ll 1$

$$\frac{\partial \bar{Q}}{\partial \bar{t}} + \frac{4}{3}\frac{Q_0T_0}{A_0L_0}\frac{\partial}{\partial \bar{x}}(\frac{\bar{Q}^2}{\bar{A}}) = -\frac{A_0K\delta RT_0}{\rho L_0Q_0}\frac{\partial \bar{R}}{\partial \bar{x}} - \frac{8\nu T_0Q}{R_0^2\bar{R}^2} \tag{26}$$

If $\alpha \gg 1$

$$\frac{\partial \bar{Q}}{\partial \bar{t}} + \frac{Q_0 T_0}{A_0 L_0} \frac{\partial}{\partial \bar{x}} (\frac{\bar{Q}^2}{\bar{A}}) = -\frac{A_0 K \delta R T_0}{\rho L_0 Q_0} \frac{\partial \bar{R}}{\partial \bar{x}} - \frac{\sqrt{2}\alpha \nu T_0 Q}{R_0^2 \bar{R}^2}. \tag{27}$$

The leading terms, which are $Q_0 T_0/(2\pi R_0 \delta R L_0)$ and $A_0 K \delta R T_0/(\rho L_0 Q_0)$ of eqs. 25, 26 and 27 are regarded as 1.0 by dominant balance of the important terms. Finally we obtained non-dimensional governing equations:

Conservation of mass:

$$\frac{\partial \bar{R}}{\partial \bar{t}} = -\frac{\partial \bar{Q}}{\partial \bar{x}} \tag{28}$$

Momentum equation:

If $\alpha \ll 1$

$$\frac{\partial \bar{Q}}{\partial \bar{t}} + \frac{4}{3} \frac{Q_0 T_0}{A_0 L_0} \frac{\partial}{\partial \bar{x}} (\frac{\bar{Q}^2}{\bar{A}}) = -\frac{\partial \bar{R}}{\partial \bar{x}} - \frac{8\nu T_0 \bar{Q}}{R_0^2 \bar{R}^2} \tag{29}$$

If $\alpha \gg 1$

$$\frac{\partial \bar{Q}}{\partial \bar{t}} + \frac{Q_0 T_0}{A_0 L_0} \frac{\partial}{\partial \bar{x}} (\frac{\bar{Q}^2}{\bar{A}}) = -\frac{\partial \bar{R}}{\partial \bar{x}} - \frac{\sqrt{2}\alpha \nu T_0 \bar{Q}}{R_0^2 \bar{R}^2}. \tag{30}$$

3.3 Moens-Korteweg equation

Two leading terms, which were mentioned in section 3.2, were multiplied to obtain the equation of propagation velocity:

$$\begin{aligned} 1 &= \frac{A_0 K \delta R T_0}{\rho L_0 Q_0} \frac{Q_0 T_0}{2\pi \delta R L_0} \\ &= \frac{T_0^2}{L_0^2} \frac{K}{2\pi\rho} \frac{\pi R_0^2}{R_0^2} \\ &= \frac{T_0^2}{L_0^2} \frac{K}{2\pi\rho} \frac{A_0}{R_0^2}. \end{aligned}$$

We defined $L_0/T_0 = c_0$ and substitution of the relation yields the well-known Moens-Korteweg equation in case of thin tube wall [2]:

$$c = \sqrt{\frac{KR_0}{2\rho_0}} = \sqrt{\frac{E}{1-\nu^2}\frac{h}{2\rho_0 R_0}}, \tag{31}$$

where the K is defined as $Eh/(R_0^2(1-\nu^2))$ The equation gives the velocity of the pulse wave as a function of the value of the elasticity of the artery. Here the Poisson's ratio ν is unknown; thus we defined $E_{est} = E/(1-\nu^2)$ in this study. Furthermore, the leading term $A_0 K \delta R T_0/(\rho L_0 Q_0) = 1$ is converted into eq. 32 by the propagation velocity:

$$\frac{\delta R}{R_0} = \frac{Q_0}{2A_0 c_0} = \varepsilon, \tag{32}$$

where ε is the change ratio of tube radius. Finaly the dimensional values R and P become:

$$R = R_0 + \delta R \bar{R} = R_0\left(1 + \varepsilon \bar{R}\right)$$
$$P = P_0 + K(R - R_0) = P_0 + 2\varepsilon\rho c^2 \bar{R}.$$

3.4 Flow simulation using non-dimensional governing equations

A. Elastic model, 1D viscous flow

We simulate the optimum pressure and flux in three kinds of flexible tubes. In case of natural rubber, maximum values of dimensional variable are as follows:

$t_0 = 0.3$ s	$Q_0 = 2.36\text{x}10^{-5}$ m^3	$R_0 = 4.0\text{x}10^{-3}$ m
$A_0 = 5.0\text{x}10^{-5}$ m^2	$L_0 = 5.4$ m	$\nu = 1.0\text{x}10^{-6}$ m^2/s

The Womersley number becomes 18.3; thus we use eqs. 25 and 26 for governing equations. In fact, the Womersley number is maybe a bit large to use those equations, we will overestimate the viscosity of the flow. However, we will see that the more dissipative phenomena comes from the wall itself not from the flow. The terms $Q_0 T_0/(A_0 L_0)$ and $8\nu T_0/R_0^2$ are defined as ε_1 and ε_ν. Substituting maximum values yield the following equations:

$$\frac{\partial \bar{R}}{\partial \bar{t}} = -\frac{\partial \bar{Q}}{\partial \bar{x}} \tag{33}$$

$$\frac{\partial \bar{Q}}{\partial \bar{t}} + \varepsilon_1 \frac{\partial}{\partial \bar{x}}(\frac{\bar{Q}^2}{\bar{A}}) = -\frac{\partial \bar{R}}{\partial \bar{x}} - \varepsilon_\nu \frac{\bar{Q}}{\bar{R}^2}, \tag{34}$$

where $\varepsilon_1 = 0.03$ and $\varepsilon_\nu = 0.15$. Since the coefficient ε_1 is small compared with ε_ν, we ignored the nonlinear term with the coefficient ε_1. The differential equations were computed by the MacCormack method [3]. The MacCormack scheme is a two step predictor-corrector technique. The characteristics are that it is three point in space, two level in time and it is second order accurate in time and in space. Here we write the govering equation in a conservative form:

$$\frac{\partial \mathbf{V}}{\partial t} + \frac{\partial \mathbf{F}}{\partial x} + \mathbf{S} = 0,$$

where $\mathbf{V} = (\bar{R}, \bar{Q})$ is the vector of dynamical variables, $\mathbf{F} = \left(\bar{Q}, \bar{R}\right)$ is the vector of conserved quantities and $\mathbf{S} = (0, \dfrac{\bar{Q}}{\bar{R}^2})$ is the sorce term. The difference equations are given by:

the predictor step

$$\mathbf{V}_i^* = \mathbf{V}_i^n - \frac{\Delta t}{\Delta x}\left(\mathbf{F}_{i+1}^n - \mathbf{F}_i^n\right) - \Delta t \mathbf{S}_i^n$$

the corrector step

$$\mathbf{V}_i^{n+1} = \frac{1}{2}\left(\mathbf{V}_i^n + \mathbf{V}_i^*\right) - \frac{\Delta t}{2\Delta x}\left(\mathbf{F}_i^* - \mathbf{F}_{i-1}^*\right) - \frac{\Delta t}{2}\mathbf{S}_i^*.$$

Input flux was set to a half cycle of a sinusoidal wave. We set to the boundary condition as follows.

$$\begin{aligned} \bar{Q}|_{x=0,L/c_0} &= 0 \\ \left.\frac{\partial \bar{R}}{\partial x}\right|_{x=0,L/c_0} &= 0. \end{aligned}$$

We then simulated the flux and pressure waves as functions of time and space. Figures 6 and 7 show the examples of the waves calculated at $\bar{x} = 0.028$, 0.95, 1.88, 2.80, 3.73 and 4.65. Here at each position $\bar{x}$ is equal to measurement positions

1-6 as shown in Fig. 2. These values are obtained from the equation $\bar{x} = L_0 x$. The results show that the amplitude decreases due to the propagation distance. Then the gradient of attenuation is in good agreement with that of analytical wave $Q = Q_0 + Q \exp(-\varepsilon_\nu \bar{x}/2)$, which is obtained from eqs. 33 and 34. However, the change of half bandwidth was not observed. Because measured waveforms contain the nonlinear effects and changes of the half bandwidth, the elastic model cannot satisfy the experimental conditions accurately.

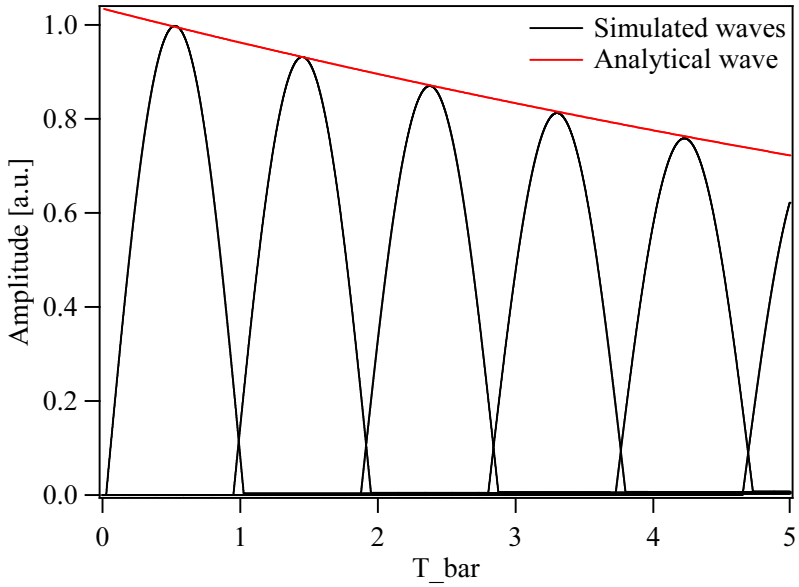

Fig. 6: Non-dimensional flux at each measurement position.

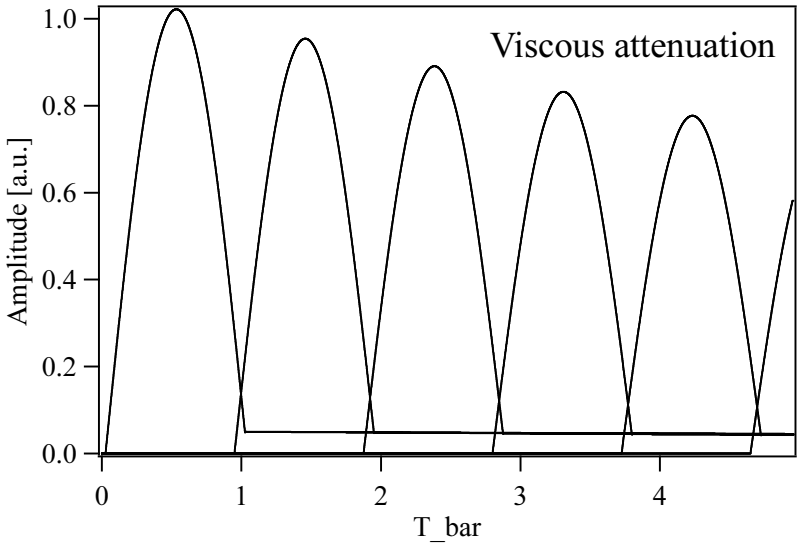

Fig. 7: Non-dimensional pressure wave at each measurement position.

B. Kelvin Voigt model, 1D viscous Flow

The Kelvin Voigt model [4] can be represented by a viscous damper and elastic spring connected in parallel and the equation is shown in eq. (35).

$$P = K\left(R - R_0\right) + \tau_\alpha \frac{\partial R}{\partial t}, \tag{35}$$

where the relaxation time τ_α is an unknown value and needed to be estimated from measurement data. Equation 33 is converted into eq. 36 using the Kelvin Voigt model instead of the elastic model:

$$\frac{\partial \bar{Q}}{\partial \bar{t}} = -\frac{\partial \bar{R}}{\partial \bar{x}} + \tau \frac{\partial^2 \bar{R}}{\partial \bar{x^2}} - \varepsilon_\nu \frac{\bar{Q}}{\bar{R}^2}. \tag{36}$$

Figures 10 and 11 show the example of flux and pressure wave with the constant $\tau = 0.15$. The increase of the attenuation and half bandwidth due to the viscous effect of tube wall were confirmed. However, like the elastic model, nonlinear effect could not be observed in this case. Thus, in the next technique, we introduce a non-linear term to estimate more accurate flux and pressure wave.

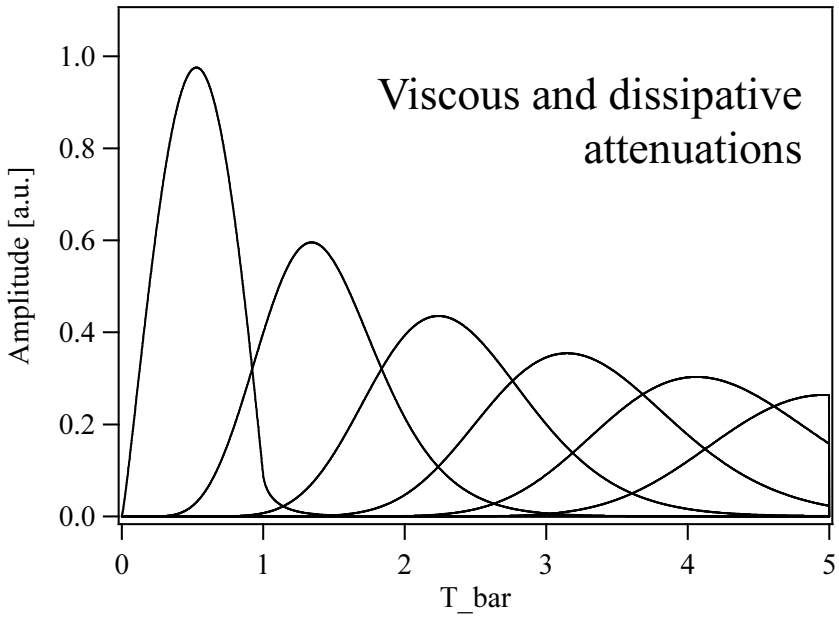

Fig. 8: Non-dimensional flux at each measurement position.

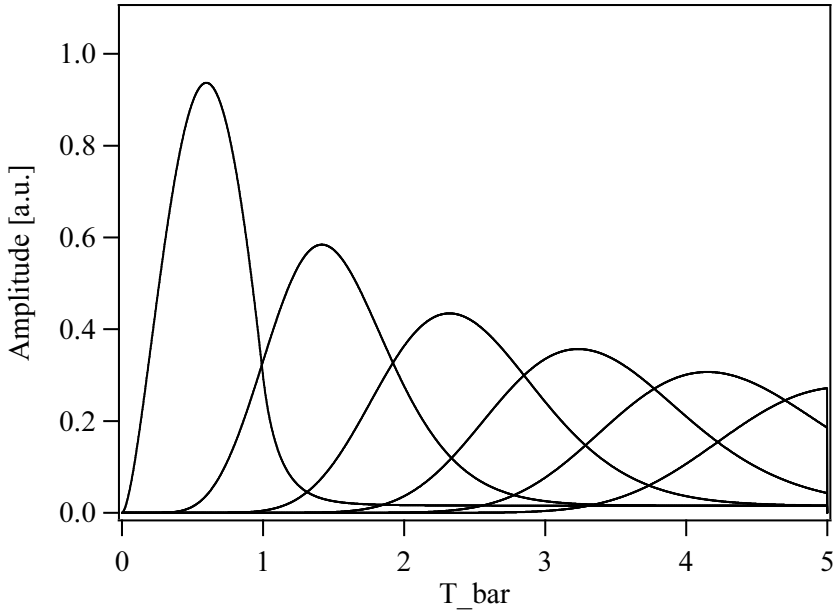

Fig. 9: Non-dimensional pressure wave at each measurement position.

C. Nonlinear effect in the tube, 1D viscous Flow

The response in displacement of the tube wall due to the pressure is nonlinear. The tube law can be represented by:

$$P = K\left((R - R_0) + \varepsilon_p (R - R_0)^2 + c_1 \varepsilon_p^2 (R - R_0)^3 + \cdots\right), \tag{37}$$

where ε_p and c_1 is a small value and coefficient. Thus we ignore the second-order terms [5] and apporoximate it by a parabolic law. Substitution of the relation in eq. 36 yields:

$$\frac{\partial \bar{Q}}{\partial \bar{t}} = -\frac{\partial}{\partial \bar{x}}(\bar{R} + \varepsilon_p \bar{R}^2) + \tau \frac{\partial^2 \bar{Q}}{\partial \bar{x}^2} - \varepsilon_\nu \frac{\bar{Q}}{\bar{R}^2} \tag{38}$$

We first tried to simulate pressure and flow waves propageting in natural rubber using a half cycle of a sinusoidal input signal. Figure 10 shows the fitting result with the coefficients $E_{est} = 950\,\mathrm{kPa}$, $\varepsilon_p = 0.15$, and $\tau = 0.03$. Here the estimated maximum pressure value was about $7\,\mathrm{kPa}$ and had error of $2\,\mathrm{kPa}$ compared with measured maximum value. For appropriate fitting, we used the maximum value obtained from the experimental data as a peak amplitude. The simulation result was not in good agreement with the measured data. This is because the input flow of pump is not a purely sinusoidal wave. Since the first mesurement point is only $0.15\,\mathrm{m}$ far from the input point, there is little nonlinear and attenuation effects on the pressure wave. Thus the pressure wave measured at the first point is almost the same as flow velocity of pump. We then introduced the wave as a input signal.

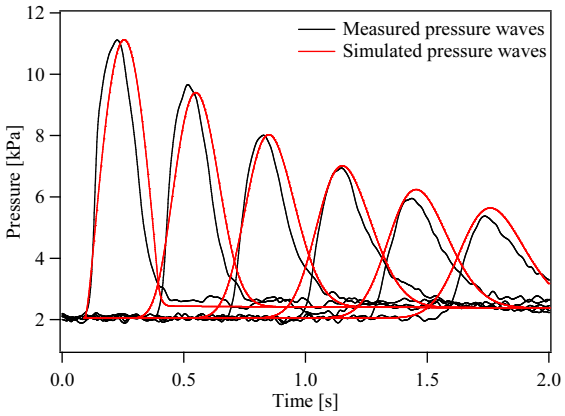

Fig. 10: Measured and simulated pressure waves A (natural rubber tube).

Selecting the appropriate coefficients E_{est}, ε_p and τ, we obtained the pressure waves propagated in the natural, silicone, and neoprene rubber tubes, which were similar with the experimental results. The optimum combinations of the coefficients are shown in table 1. The term E_{msr} means the elastic modulus measured by a stress-strain test. There are the differences between data. This comes from the fact that the relation between E and $K(= Eh/(R_0^2(1-\nu^2)))$ is not so simple as we think because the thickness of the tube walls are thick (2 mm). Then the comparison between the measured and simulated pressure waves are shown in Figs 11, 12, and 13. The simulation results were in good agreement with the measured datas. However, we could not tell the estimation accuracy of waveforms. Therefore, it is necessary to introduce the cost function which calculates the difference between measured and estimated results for further analysis [5].

	E_{msr} [MPa]	E_{est} [MPa]	ε_p	τ
Natural rubber	1.3	1.0	0.10	0.025
Silicone rubber	2.5	3.8	0.08	0.045
Neoprene rubber	4.6	4.7	0.10	0.043

Table 1: Optimum combination of parameters.

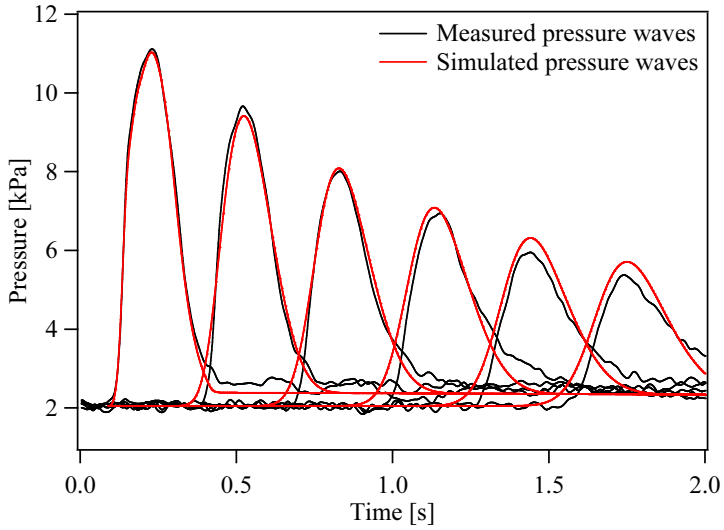

Fig. 11: Measured and simulated pressure waves B (natural rubber tube).

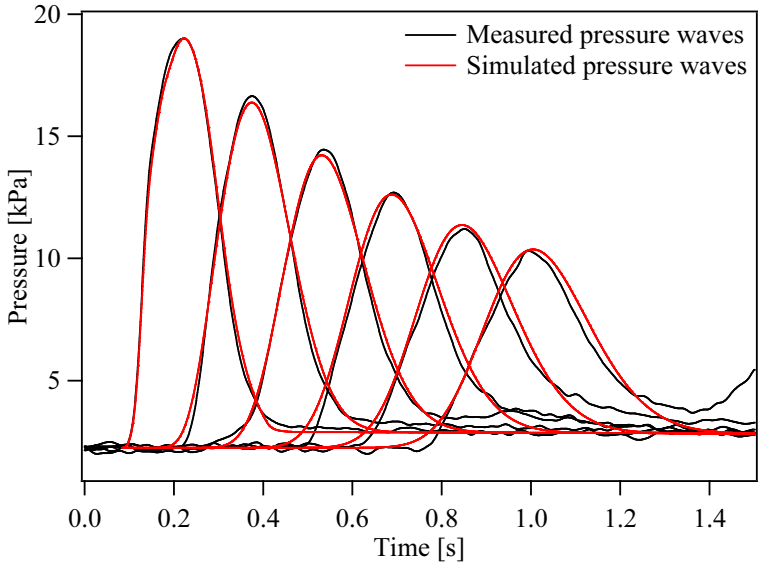

Fig. 12: Measured and simulated pressure waves (silicone rubber tube).

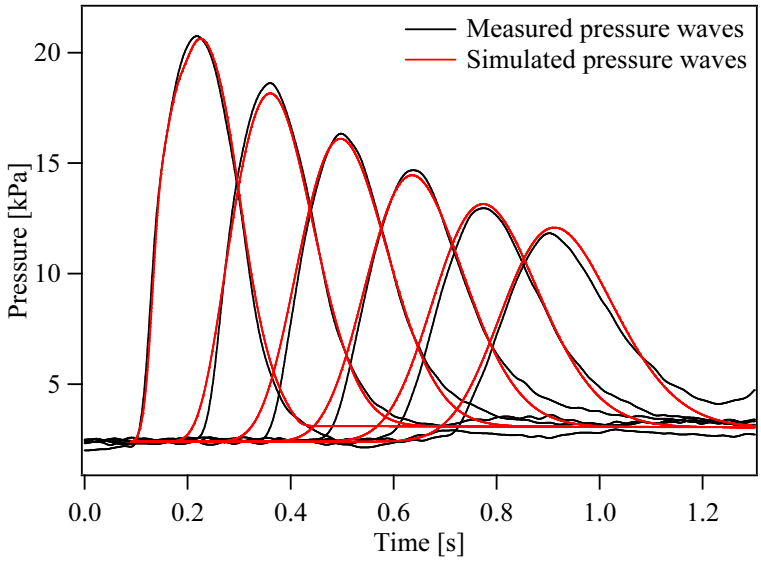

Fig. 13: Measured and simulated pressure waves (neoprene rubber tube).

3.5 Accuracy of one-dimensional equations

We cross checked the accuracy of the simple one-domensional governing equations by a commercial Finite Element Method (FEM) software COMSOL 3.4, which solves full Navier-Stokes equations.
We simulated the pressure waves propagating in the natural rubber tube using one-dimension model and COMSOL and compared the results. The length, radius, and thickness of the tube model are $10\ \mathrm{m}$, $4.0\ \mathrm{mm}$, and $2.0\ \mathrm{mm}$, respectively. Input signal was a half cycle of sinusoid wave with time interval $0.3\ \mathrm{s}$. Input fluid was water (density $1000\ \mathrm{kg/m^3}$). Governing equations were conservation of mass and momentum equation as shown in eqs. 32 and 37. The optimum parameters are obtained from the previous flow simulation (Table 1). Finally the pressures at positions $x = 0.15$, 2.65, 5.15, and 7.65 were calculated by MacCormack scheme.
In case of COMSOL, the computations were done using a 2D axial-symmetric stress-strain mode. Governing equations used were full Navier-Stokes equations shown in eqs. 1, 2, and 3. For stress-strain analysis, the elasticity equations expressed as $\nabla \bullet \sigma_{ij} = \mathbf{F}$ was used. Here σ and $\mathbf{F}$ denote the stress tensor and the volume forces. Then arbitrary Lagrangian-Eulerian (ALE) method makes it possible to simulate the deformation of tube wall. We used coarse and fine meshs shown in Fig. 14 for the FEM computation. Actually we could not calculated using more fine mesh because of time-consuming and lack of memory. The material was assumed to be elastic body with the elasticity = $1.9\ \mathrm{MPa}$, density = $400\ \mathrm{kg/m^3}$ and Poisson's ratio = 0.45. The viscous attenuation was calculated by the Rayleigh damping model which describe the solid motion with viscous damping and with a single degree of freedom by:

$$m\frac{d^2u}{dt^2} + \xi\frac{du}{dt} + ku = f(t), \tag{39}$$

where u is the displacement, m the mass, k the stiffness coefficient, and ξ the damping parameter given by $\xi = \alpha_{dM} + \beta_{dk}k$. α_{dM} and $\beta_{dk}k$ are automatically set [6].
Figure 15 shows the pressures calculated by one-dimension model and COMSOL. There is little difference among waveforms, telling us that simple one-dimensional equations can simulate the same results obtained from full Navier-Stokes equations. The difference thing is the computation time. In case of COMSOL, it took two hours for the pressure calculating in coase mesh, six hours for that in fine mesh. For the time computed by the one-dimensional mode, it took only a few second. Therefore, the simple one-dimensional model is useful for simulating the

flow dynamics in flexible tubes. However, we should pay attention to the decision of parameters in case of one-dimensional model because the wall elasticity in case of COMSOL is about twice as big as that of one-dimensional model. One reason is the other is longitudinal effect is neglected in case of one-dimension model.

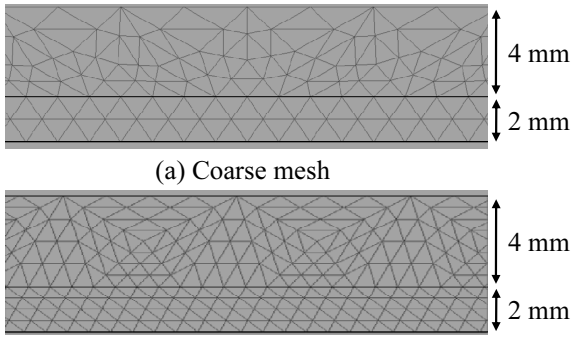

Fig. 14: Mesh configuration.

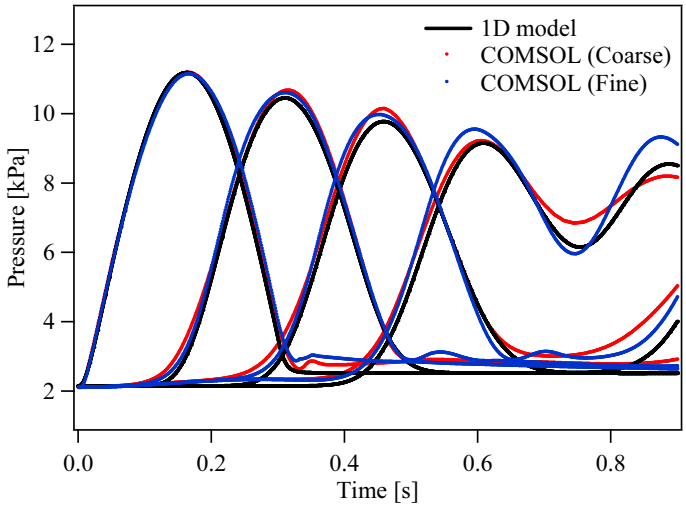

Fig. 15: Simulated pressure waves.

4 Flow simulation in various forms and characteristics of tube

In this section, we derive non-dimensional governing equations for flow simulation in the tubes with different inner diameter, wall elasticity, and thickness. Then the bifurcation simulation model is also derived.

4.1 Flow simulation in a straight tube with different characteristics

Let us come back to the mathematical modelisation:

Conservation of mass:

$$\frac{\partial A}{\partial t} + \frac{\partial Q}{\partial x} = 0.$$

Momentum equation:

If $\alpha \ll 1$

$$\frac{\partial Q}{\partial t} + \frac{4}{3}\frac{\partial}{\partial x}\left(\frac{Q^2}{A}\right) = -\frac{A}{\rho}\frac{\partial p}{\partial x} - \frac{8\nu Q}{R^2}$$

If $\alpha \gg 1$

$$\frac{\partial Q}{\partial t} + \frac{\partial}{\partial x}\left(\frac{Q^2}{A}\right) = -\frac{A}{\rho}\frac{\partial p}{\partial x} - \frac{\sqrt{2}\alpha\nu Q}{R^2}.$$

Pressure law (Voigt model, Nonlinear term):

$$P = P_0 + K\left((R - R_0) + \varepsilon(R - R_0)^2\right) + \eta\frac{\partial R}{\partial t}.$$

For simulating the fluid dynamics in the tubes with different inner diameter, wall elasticity, and thickness, we introduce dimensional variables as shown below:

$$t = T_0\bar{t} \qquad x = L_0\bar{x} \qquad Q = Q_0\bar{Q} \qquad h = h_0\bar{h} \qquad E = E_0\bar{E}$$

$$R = R_0\bar{R_{df}} + \delta R\bar{R} \qquad A = A_0\bar{A} = \pi R_0^2\left(\bar{R_{df}}^2 + 2\frac{\delta R}{R_0}\bar{R}\right)$$

$$K = \frac{Eh}{R^2} = \frac{E_0 h_0}{R_0^2}\frac{\bar{E}\bar{h}}{\bar{R_{df}^2}} = K_0\bar{K}$$

where $\bar{R_{df}}$, $\bar{E}$, $\bar{h}$, and $\bar{K}$ show the changes of the tube. Substituting variables and pressure law into conservation of mass and momentum equation yields:

Conservation of mass:

$$\bar{R_{df}}\frac{\partial \bar{R}}{\partial \bar{t}} = -\frac{Q_0 T_0}{2\pi R_0 \delta R L_0}\frac{\partial \bar{Q}}{\partial \bar{x}}. \tag{40}$$

Momentum equation:

If $\alpha \ll 1$

$$\frac{\partial \bar{Q}}{\partial \bar{t}} + \frac{4}{3}\frac{Q_0 T_0}{A_0 L_0}\frac{\partial}{\partial \bar{x}}(\frac{\bar{Q}^2}{\bar{R}_{df}^2}) = \\ -\frac{A_0 K_0 \delta R T_0}{\rho L_0 Q_0}\left(\frac{\partial(\bar{K}\bar{R})}{\partial \bar{x}} + \varepsilon \delta R \frac{\partial(\bar{K}\bar{R}^2)}{\partial \bar{x}} - \frac{\eta}{K_0 T_0}\bar{R_d} f \frac{\partial^2 \bar{Q}}{\partial \bar{x}^2}\right) - \frac{8\nu T_0 \bar{Q}}{R_0^2 \bar{R_{df}^2}} \tag{41}$$

If $\alpha \gg 1$

$$\frac{\partial \bar{Q}}{\partial \bar{t}} + \frac{Q_0 T_0}{A_0 L_0}\frac{\partial}{\partial \bar{x}}(\frac{\bar{Q}^2}{\bar{R}_{df}^2}) = \\ -\frac{A_0 K_0 \delta R T_0}{\rho L_0 Q_0}\left(\frac{\partial(\bar{K}\bar{R})}{\partial \bar{x}} + \varepsilon \delta R \frac{\partial(\bar{K}\bar{R}^2)}{\partial \bar{x}} - \frac{\eta}{K_0 T_0}\bar{R_d} f \frac{\partial^2 \bar{Q}}{\partial \bar{x}^2}\right) - \frac{\sqrt{2}\alpha \nu T_0 Q}{R_0^2 \bar{R_{df}^2}}. \tag{42}$$

The leading terms, which are $Q_0 T_0/(2\pi R_0 \delta R L_0)$ and $A_0 K_0 \delta R T_0/(\rho L_0 Q_0)$ of eqs. 40, 41 and 42 are regarded as 1.0. Finally we obtained non-dimensional governing equations:

Conservation of mass:

$$\bar{R_{df}}\frac{\partial \bar{R}}{\partial \bar{t}} = -\frac{\partial \bar{Q}}{\partial \bar{x}}. \tag{43}$$

Momentum equation:

If $\alpha \ll 1$

$$\frac{\partial \bar{Q}}{\partial \bar{t}} + \frac{4}{3}\frac{Q_0 T_0}{A_0 L_0}\frac{\partial}{\partial \bar{x}}(\frac{\bar{Q}^2}{\bar{R}_{df}^2}) = -\frac{\partial(\bar{K}\bar{R})}{\partial \bar{x}} - \varepsilon_p \frac{\partial(\bar{K}\bar{R}^2)}{\partial \bar{x}} + \tau \bar{R_{df}}\frac{\partial^2 \bar{Q}}{\partial \bar{x}^2} - \frac{8\nu T_0 \bar{Q}}{R_0^2 \bar{R_{df}^2}} \tag{44}$$

If $\alpha \gg 1$

$$\frac{\partial \bar{Q}}{\partial \bar{t}} + \frac{Q_0 T_0}{A_0 L_0} \frac{\partial}{\partial \bar{x}} (\frac{\bar{Q}^2}{\bar{R}_{df}^2}) = -\frac{\partial (\bar{K}\bar{R})}{\partial \bar{x}} - \varepsilon_p \frac{\partial (\bar{K}\bar{R}^2)}{\partial \bar{x}} + \tau \bar{R_{df}} \frac{\partial^2 \bar{Q}}{\partial \bar{x}^2} - \frac{\sqrt{2}\alpha\nu T_0 Q}{R_0^2 \bar{R_{df}^2}}, \quad (45)$$

with parameters given by $\varepsilon_p = \varepsilon\delta R$ and $\tau = \eta/(K_0 T_0)$.
We then simulated pressures in the tube with different radius and elasticity as shown in Fig 16. Here we assumed nonlinear and friction terms of Navier stokes equation, ε_p and τ are zero for simple computation. The result is shown in Fig. 17. We confirmed the reflected wave was caused at discrete transition. The propagation velocities did not change in both domains, because the velocity calculated by the Moens-Korteweg equation $\sqrt{Eh/2\rho R}$ did not change. Then the amplitude of reflected and transmitted waves became 0.6 and 1.6, respectively, after reflection. This phenomenon is expressed by the admittance of tube. Generally, the reflection coefficient R and the transmission coefficient T of pressure are defined as the following expressions [1]:

$$R = \frac{P_r}{P_i} = \frac{Y_0 - Y_1}{Y_0 + Y_1} \quad (46)$$

$$T = \frac{P_t}{P_i} = \frac{2Y_0}{Y_0 + Y_1}, \quad (47)$$

with the admittance written as:

$$Y = \frac{A}{\rho c}, \quad (48)$$

where suffixes i, r, and t mean the incident, reflected, and transmitted waves. Y_0 and Y_1 are admittance at left and right domain. In this case, only cross section changed from A_0 to $0.25A_0$. Thus the reflection and transmission coefficients are 0.6 and 1.6. These values were the same as the results obtained from simulated data. Therefore it is possible to simulate the pressure in the tube with different forms and characteristics by obtained governing equations.

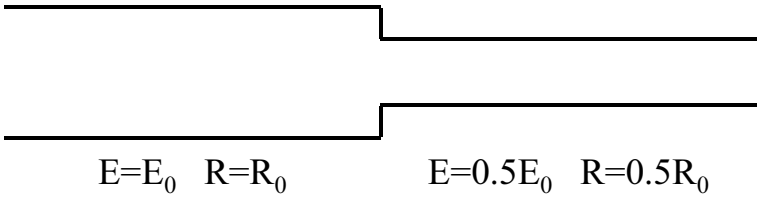

Fig. 16: Simulation model with different radius and elasticity.

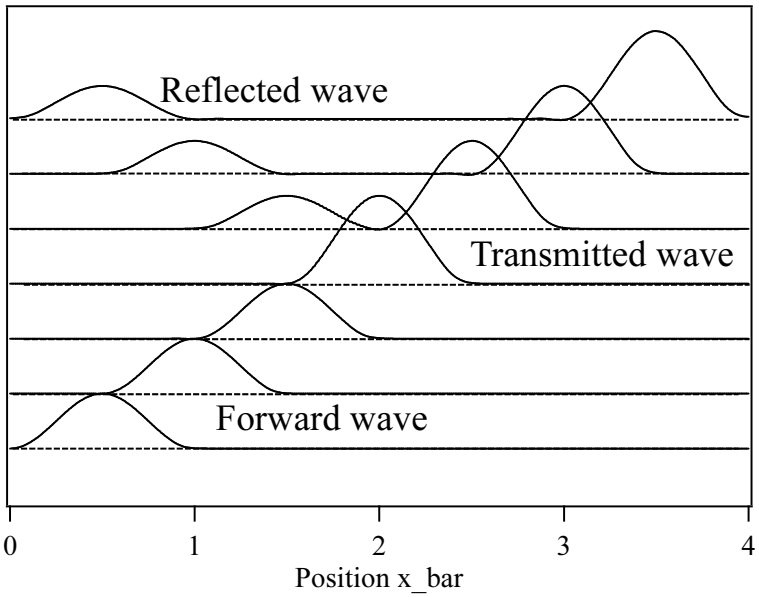

Fig. 17: Generation of reflected wave.

4.2 Flow simulation in a bifurcation model

This section describes the simulation in bifurcation tube as shown in Fig. 18. The governing equations are the same as ones used in section 4.1. The differential equations are computed by the MacCormack method. The important thing is boundary conditions at a bifurcation. Figure 19 shows the discrete values of radius and flow velocities in the mother and daughter tubes. Here the superscripts A and B mean the daughter tube A and B, respectively. The subscripts mean the positions in tubes. In predictor step, we calculated R which is the radius at the bifurcation point using the following expression:

$$R = \frac{1}{3}\left(R_{n-1} + R_1^A + R_1^B\right). \tag{49}$$

Here we assumed the pressure loss at the point and the effect of daughter tube's angle to the mother tube could be negligible. In corrector step, we decide the flux satisfies the conservation of mass expressed as $Q = Q_1 + Q_2$ at the bifurcation [7] (See Fig. 18). The term Q is the flux propagating in the mother tube, Q_1 and Q_2 are those in the daughter tubes. Furthermore, we assume nonlinear and friction terms of eq. 44, ε_p, and τ are zero for a simple computation. From these assumptions and conservation of mass, the boundary condition of flux is decided as follows:

$$Q_n = \frac{1}{3}(2Q_1 + Q_1^A + Q_1^B) \tag{50}$$

$$Q_0^A = \frac{1}{3}(Q_1 + 2Q_1^A - Q_1^B) \tag{51}$$

$$Q_0^B = \frac{1}{3}(Q_1 - Q_1^A + 2Q_1^B). \tag{52}$$

We then simulated pressures in the bifurcation model. Figure 20 shows the simulation result. One can observe the wave reflection is caused by the bifurcation point, and a wave speed becomes slightly higher in the branch with smallest radius. We confirmed wave velocity and the maximum amplitude follow, respectively, the Moens-Korteweg equation and the reflection and transmission coefficients which are given by [1]:

$$R = \frac{P_r}{P_i} = \frac{Y_0 - (Y_1 + Y_2)}{Y_0 + (Y_1 + Y_2)} \tag{53}$$

$$T = \frac{P_t}{P_i} = \frac{2Y_0}{Y_0 + (Y_1 + Y_2)}. \tag{54}$$

where Y_0 is the admittance of the mathor tube, Y_1 and Y_2 are those of daughter tubes. Therefore, it is possible to simulate the pressure in bifurcation model simply by the governing equations and boundary condition.

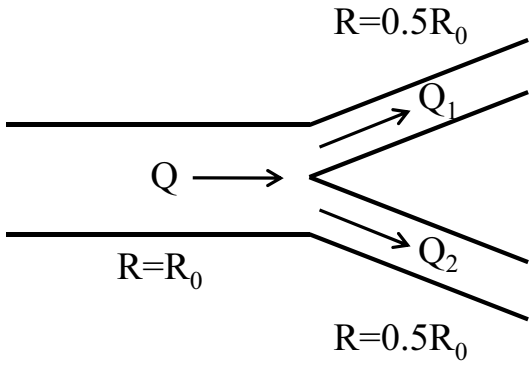

Fig. 18: A bifurcation model.

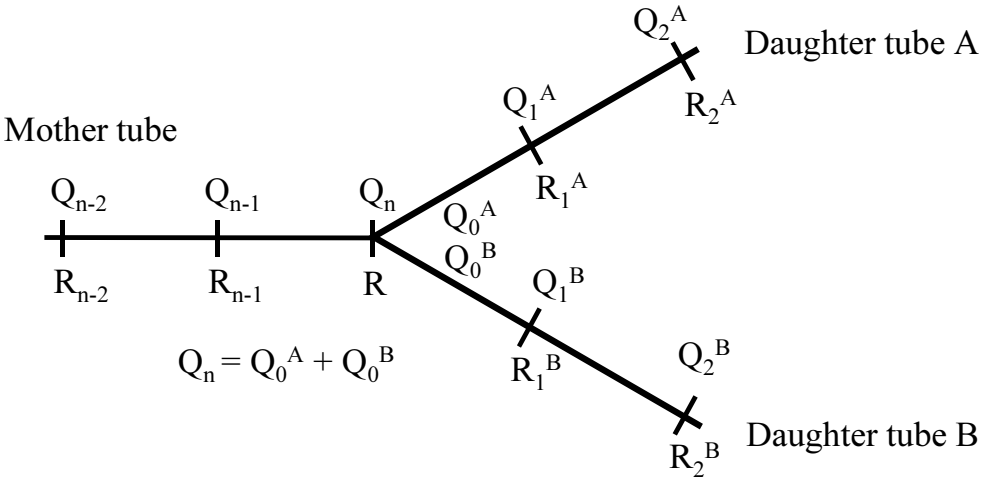

Fig. 19: Discrete values of radii and flow velocities in mother and daughter tubes.

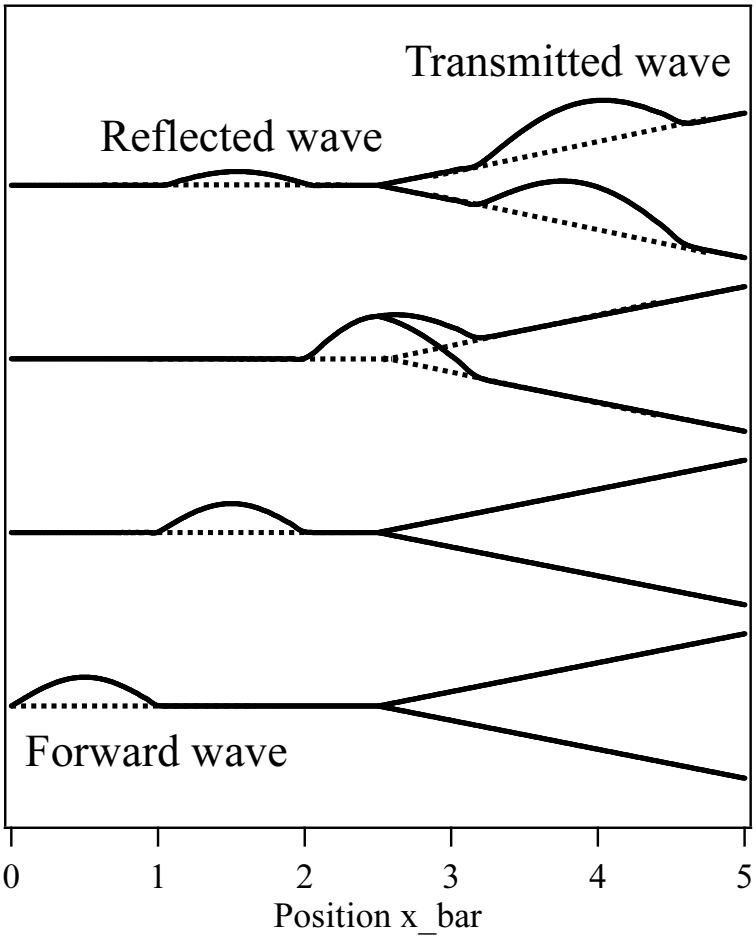

Fig. 20: Simulated pressure waves propagating in the bifurcation model.

5 Measurement and simulation of fluid dynamics in the simple human artery model

In this section, we measure the flow velocity and pressure waves in a simple human artery model. Then we build the model by combining two bifurcation models expressed in previous section, and simulate the flow dynamics in it. Finaly we compare the results.

5.1 Experiment

Figure 21 shows the details of a simple human artery model, with central artery, femoral artery and carotid artery. Viscoelastic tubes (Custom made, Polyurethane) are used for each artery. The elastic modulus of the polyurethane was about 70 kPa by the tensile test. Propagation velocity of the intravascular pressure wave in this tube was near the pulse wave velocity in vivo. Diameter of the tube changes from 10 to 6 mm from the pump to the tank. The length is based on the size of human artery.

A measurement system was constructed by a pump (Custom made, Tomita engineering Co., Ltd), the simple human artery model, and three tanks (Fig. 22). A pulse flow was input into the human artery model from the pump. The input signal to the pump was a half cycle of a sinusoidal wave with time interval of 0.3 sec. The total flow volume was 4.5 ml. We measured the inner pressure wave and flow velocity in the human artery model. Measurement point was set at 170 mm from first bifurcation to tank 1. This point is assumed as the carotid artery of neck in an actual human body. We used a pressure sensor (Keyence AP-10S) to measure inner pressure wave. We used ultrasonic Doppler system (Toshiba Medical Systems Aplio SSA-700A) to measure flow velocity. The center frequency of the ultrasonic pulse used (Toshiba Medical Systems Probe PLT-1204AT) was 12 MHz.

Figure 23 shows measured results of normalized inner pressure wave and flow velocity.

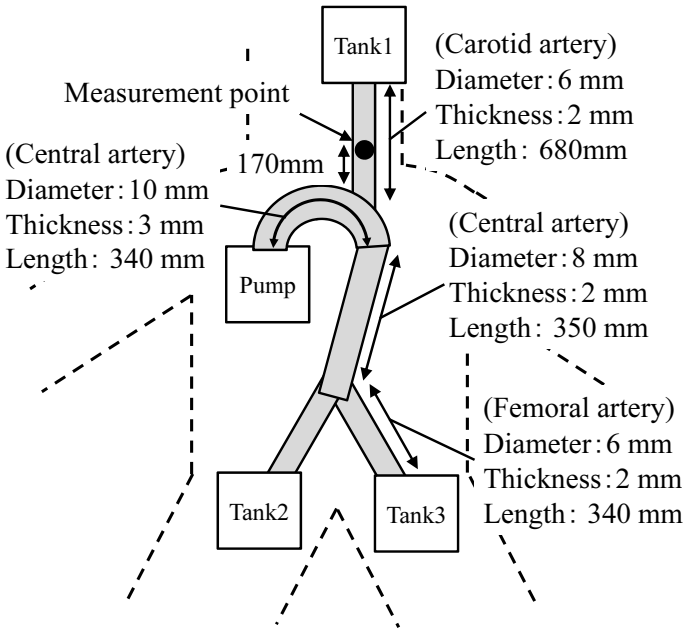

Fig. 21: Details of the simple human artery model.

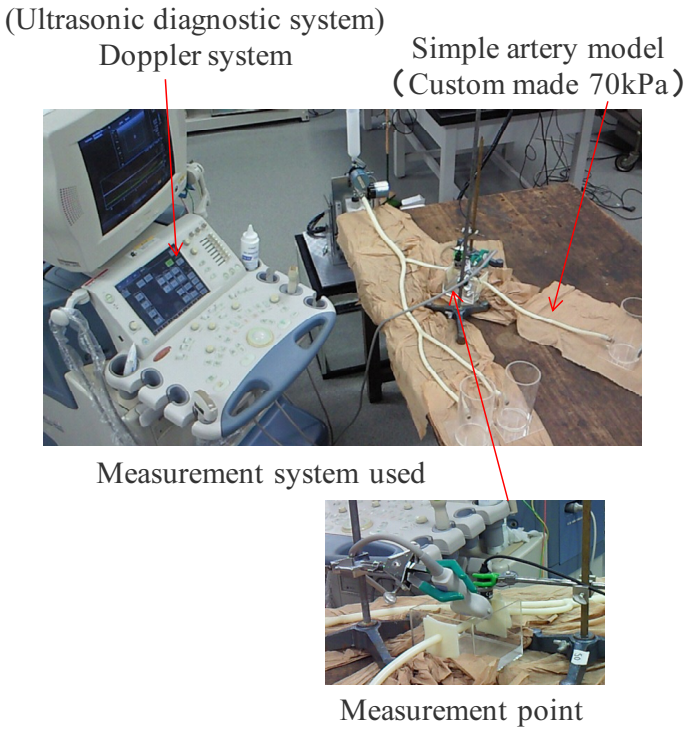

Fig. 22: Measurement system used.

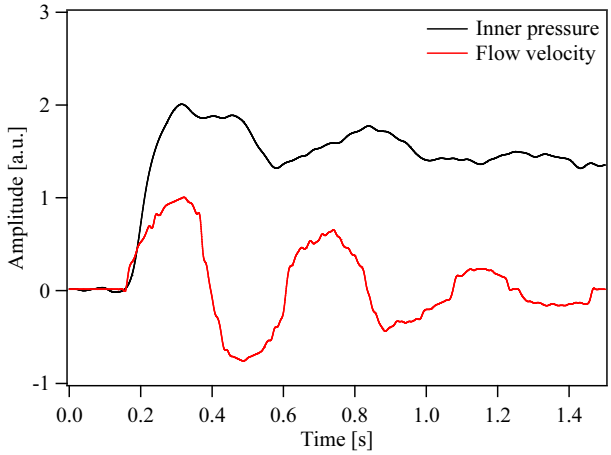

Fig. 23: Observed inner pressure wave and flow velocity.

5.2 Simulation and comparison of the results

We first explain the simulation details. The model definitions are shown in Fig. 21. We build the simple artery simulation model by combining two bifurcation models with the boundary condition at the bifurcation points. We set another boundary condition causing the fully reflection at the end of tubes. The Womersley numbers calculated from the details of five tubes are less than 22.8; thus we used the govering equations in case of small α shown in eqs. 43 and 44. In fact, the Womersley number is maybe a bit large to use those equations, we will overestimate the viscosity of the flow. However, we have seen that the more dissipative phenomena came from the wall itself not from the flow. We assume the nonlinearity of Navier-Stokes equation can be neglected for simple analysis because the estimated value is less than 3 %. Changing the values of elasticity E, relaxation time τ, and nonlinearity of tube wall ε_p, we decide the optimum values. The results with $E = 63$ kPa, $\tau = 0.06$, and $\varepsilon_p = 0.15$ are shown in Figs. 24 and 25. The amplitudes are normalized. In consequence, the simulated flow velocity was in good agreement with the measured data, while the estimated pressure has large error. However, the trend of variation of pressure is well predicted. The change in mean pressure is maybe due to the fact that there is more water in the final model so that the deformation has changed. Furthermore, the actual flow velocity and pressure waves are more complex than the simulated waves. It seems that the waves contain other reflected waves in additional to the reflected waves at the end of tubes. However, we find several similarities in flow velocity waves. Therefore, the results tell us the possibility of human artery model simulation using this simple one-dimension technique.

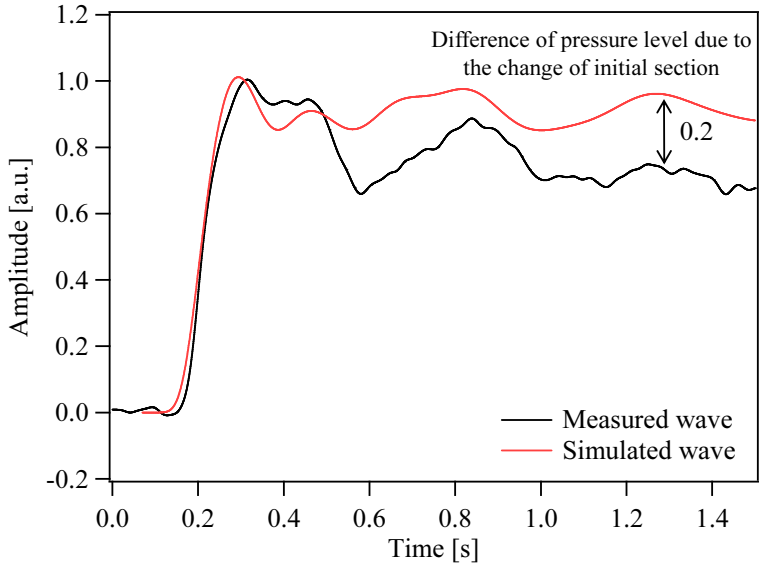

Fig. 24: Measured and simulated pressure waves in a simple human artery model.

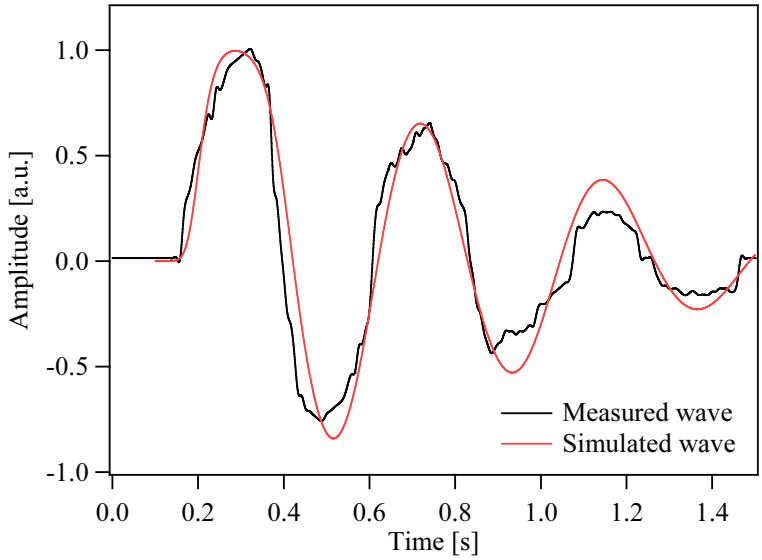

Fig. 25: Measured and simulated flow velocities in a simple human artery model.

6 Conclusion

We first considered the steady and periodic flow in a rigid tube to obtain simple velocity profiles which depend on the Womersley number. We then derived the simple one-dimensional governing equations in cases of small and large Womersley numbers for the flow simulations in the straight viscoelastic tube.
In chapter 3, we measured the pressures in three kinds of viscoelastic tubes, and simulate the flow propagation using the Kelvin-Voigt and nonlinear models. In consequence, the estimated pressures were in good accordance with the estimation. Then the estimated elasticity were near the measured values. However, we should pay attention to the decision of parameters. Therefore, it is necessary to introduce the cost function to calculate the difference between measured and estimated results for further analysis.
In chapters 4 and 5, we constructed the human artery model and measured the inner pressures and flow velocity. Then we built the same simulation model using the bifurcation model and simulate the flow dynamics. As a result, the result is not satisfactory for the pressure, but it is for the flow velocity. Since the measured pressure and flow velocity waves contain many reflected waves in additional to those from the end of tubes, we should evaluate the cause of the difference in detail. Futuremore, we need to investigate the effective simulation model combination such as the generalized Voigt, with consideration of Maxwell models or other nonlinear terms.

Acknowledgement

In any project there occurs times where assistance is much appreciated, To this end, I wish to express my sincere thanks to the following people.
For their kind support, I would like to acknowledge Mr. Yuya Yamamoto for the assistance with experiments and suggestions. I also wish to acknowledge Associate Prof. Shintaro Takeuchi at Osaka university. I would also like to thank Prof. Patrice Flaud at Université Paris Diderot for valuable discussions of flow dynamics in human artery.
On the discussion of one-dimensional simulation technique, I would like to thank Prof. José Maria Fullana at Université Pierre et Marie-Curie.
I must greatly thank Prof. Mami Matsukawa at Doshisha University for giving me the opportunity to come in France and valuable discussions of ultrasonic experiment procedure.
I also wish to express my gratitude to Ms. Audrey Gineau for her kind encouragement and valuable comments throught this project.
Finally and most importantly, I wish to express my sincere thanks to Prof. Pierre-Yves Lagrée at Université Pierre et Marie-Curie, for his continuous heartwarming encouragement and various helpful discussions. Not only for this study but also for the whole field of science, I wish to acknowledge that his precious advice always supported me throughout the daily studies.

References

[1] Van de Vosse and Van Dongen: Cardiovascular Fluid Mechanics -lecture notes (Eindhoven University of Technology, faculty of Mechanical Engineering, faculty of Applied Physics, 1998).

[2] Pedley: The Fluid Mechanics of Large Blood Vessels (Cambridge University Press, Cambridge, 1980)

[3] Jose-Maria Fullana and Stéphan Zaleski: A branched one-dimensionamodel of vessel networks, J. Fluid Mech. **621** (2009) 183-204.

[4] T. Nakagawa and H. Kanbe: Rheology (Misuzu, Tokyo, 1959) p. 361 [in Japanese].

[5] Pierre-Yves Lagrée: An inverse technique to deduce the elasticiy of a large artery, Eur. Phys. J. AP. **9** (2000) 153-163.

[6] Comsol HELP Chapter 8 and 14, Modeling guid.

[7] Olufsen MS, Peskin CS, Kim WY, Pedersen EM, Nadim A, and Larsen J: Numerical simulation and experimental validation of blood flow in arteries with structured-tree outflow conditions, Ann. Biomed. Eng. **28(11)** (2000) 1281-1299.